The fate of fluvially-deposited organic carbon during transient floodplain storage

Scheingross, J.S.[1,2*], Repasch, M.N.[1,3], Hovius, N[1,3], Sachse, D.[1], Lupker, M.[4], Fuchs, M.[5], Halevy, I.[6], Gröcke, D.R.[7], Golombek, N.Y.[1,3,8], Haghipour, N.[4,9], Eglinton, T.I.[4], Orfeo, O[10], Schleicher, A.M.[1]

[1] GFZ-German Research Centre for Geosciences, Potsdam, Germany
[2] Department of Geological Sciences and Engineering, University of Nevada Reno, USA
[3] Institute of Geosciences, University of Potsdam, Germany
[4] Geological Institute, ETH Zürich, Zürich, Switzerland
[5] Helmholtz-Zentrum Dresden-Rossendorf, Helmholtz Institute Freiberg for Resource Technology, Germany
[6] Department of Earth and Planetary Sciences, Weizmann Institute of Science, Rehovot, Israel
[7] Department of Earth Sciences, Durham University, Durham, UK
[8] Department of Earth and Environmental Sciences, Dalhousie University, Halifax, Canada
[9] Laboratory of Ion Beam Physics, ETH Zürich, Zürich, Switzerland
[10] Centro de Ecología Aplicada del Litoral, CONICET, Corrientes, Argentina
*Corresponding author (jscheingross@unr.edu)

Abstract

CO_2 release from particulate organic carbon (POC) oxidation during fluvial transit can influence climate over a range of timescales. Identifying the mechanistic controls on such carbon fluxes requires determining where POC oxidation occurs in river systems. While field data show POC oxidation and replacement moving downstream in lowland rivers, flume studies show that oxidation during active fluvial transport is limited. This suggests that most fluvial POC oxidation occurs during transient floodplain storage, but this idea has yet to be tested. Here, we isolate the influence of floodplain storage time on POC oxidation by exploiting a chronosequence of floodplain deposits above the modern groundwater table in the Rio Bermejo, Argentina. Measurements from 15 floodplain cores with depositional ages from 1 y to 20 ky show a progressive POC concentration decrease and ^{13}C-enrichment with increasing time spent in floodplain storage. These results from the Rio Bermejo indicate that over 80% of fluvially-deposited POC can be oxidized over millennial timescales in aerated floodplains. Furthermore, POC in the oldest floodplain cores is more ^{14}C-enriched than expected based on the

independently-dated floodplain ages, indicating that a portion of this oxidized POC is replaced by autochthonous POC produced primarily by floodplain vegetation. We suggest floodplain storage timescales control the extent of oxidation of fluvially-deposited POC, and may play a prominent role in determining if rivers are significant atmospheric CO_2 sources.

Introduction

Lowland river systems influence the geologic carbon cycle via the production, transfer, and oxidation of particulate organic carbon (POC) (e.g., Bianchi et al., 2018; Hilton and West, 2020). POC sourced from the terrestrial biosphere (POC_{bio}) that escapes oxidation during fluvial transit can be buried in marine sediments, providing a long term CO_2 sink and O_2 source, whereas POC sourced from erosion of sedimentary rock (POC_{petro}) can release CO_2 to the atmosphere and consume O_2 via oxidation during exhumation and fluvial transit (e.g., Galy et al., 2008a; Hemingway et al., 2018; Hilton and West, 2020).

Whether lowland rivers act as net sources or sinks of atmospheric CO_2 over geologic timescales depends on the source and fate of POC during fluvial transit as well as inorganic processes such as silicate and carbonate weathering (Hilton and West, 2020). Efficient oxidation of POC during transit through lowland rivers can push rivers towards being atmospheric CO_2 sources because oxidation of POC_{petro} directly transfers carbon from the rock reservoir to the atmosphere, and oxidation of POC_{bio} reduces the flux of recently photosynthesized carbon from the atmosphere to sedimentary basins. In contrast, if POC is stable during source to sink transport, rivers can contribute to the removal of CO_2 from the atmosphere, as the preservation of POC_{bio} increases the flux of recently photosynthesized carbon to depositional basins where it can be incorporated into geologic storage.

As POC travels downstream, it spends the majority of its total transit time in transient floodplain storage (Bradley and Tucker, 2013; Repasch et al., 2020; Torres et al., 2020; Torres et al., 2017). Together, long floodplain storage timescales and experimental evidence of negligible POC oxidation during in-river transport (Scheingross et al., 2019) suggest that the ability of POC to survive episodes of transient floodplain storage, as well as the relative proportions of POC_{bio} and POC_{petro}, may control whether lowland rivers act as atmospheric CO_2 sources or sinks. However, existing data on POC storage and oxidation in floodplains is difficult to interpret, as floodplains contain both fluvially-deposited (allochthonous) POC, and POC produced *in situ* via vegetation growth (autochthonous POC). The conflation of these two POC sources makes it difficult to discern the principal controls on the fluvial carbon budget during source to sink transit.

Floodplains are often argued to be areas of POC preservation, both due to empirical observations of carbon storage in vegetation (e.g., Hoffmann et al., 2009), and mechanistic considerations that the delivery of nutrients and fine sediment to floodplains allows efficient organic matter stabilization and autochthonous POC production (Cierjacks et al., 2010; Hoffmann et al., 2009; Lawrence et al., 2015; Zehetner et al., 2009). These arguments apply primarily to autochthonous POC preservation, and thus are valid for geologically-short residence times ($<\sim10^5$ y) of individual floodplain deposits. Arguments for floodplains to preserve allochthonous POC, and thereby sequester CO_2 over 10^6-y timescales, often cite the aging of POC_{bio} in river sediment (e.g., Galy and Eglinton, 2011; Lininger et al., 2019; Marwick et al., 2015; Torres et al., 2020). These data suggest that not all POC deposited in floodplains can be fully mineralized over existing storage timescales, which may be mechanistically explained via chemical stabilization of POC following interactions with mineral-rich sediment (Hemingway et al., 2019; Lawrence et al., 2015; Masiello et al., 2004). However, data also show POC loss and modification during downstream transport (e.g., Aufdenkampe et al., 2007; Bouchez et al., 2010; Galy et al., 2008a; Galy et al., 2008b), suggesting that at least some allochthonous POC must be oxidized during fluvial transit.

Well-constrained chronosequences provide a method to assess the fate of POC during floodplain storage. Most chronosequence studies have focused on soil development over a parent bedrock or non-fluvially deposited material, and thus do not contain the fluvially-deposited, allochthonous POC we seek to examine (e.g., Masiello et al., 2004; Schlesinger, 1990). Chronosequence studies specifically examining floodplains are often limited to only the top ~1 m of the deposit (e.g., Baisden et al., 2002; Zehetner et al., 2009). Such shallow depths are dominated by autochthonous POC (Lawrence et al., 2015; Lininger et al., 2018; Zehetner et al., 2009), making it difficult to evaluate allochthonous POC oxidation.

The limited cases in which POC fate in floodplain deposits has been examined at depths >~1 m, where allochthonous POC may be more strongly represented, show inconsistent results. An analysis of floodplain deposits up to 6 m depth within the Colorado River Basin, USA suggests POC is preserved in floodplains, but analyses were limited to depths below the groundwater table characterized by saturated, anoxic conditions (Boye et al., 2017). In contrast, comparing floodplain deposits up to ~3.5 m depth from an active floodplain and a Pleistocene terrace of the Fly River, Papua New Guinea show a loss of POC with time, suggesting ongoing POC oxidation (Goñi et al., 2014). Along the Cowlitz River, USA, a 1.2 My chronosequence with cores extracting material from up to ~4 m depth shows no clear relationship between floodplain age and POC content, but changes in the mineralogy, chemistry, and mineral surface area of the deposits with time suggest that when present, POC can be stabilized during storage (Lawrence et al., 2015). None of these studies explicitly separate allochthonous and autochthonous POC, making it difficult to assess allochthonous POC oxidation. Lacking additional data, models of POC loss during floodplain storage have assumed exponential decay with unconstrained rate parameters (Torres et al., 2017), yielding results that have yet to be field-verified.

Here, we use field measurements to assess oxidation and modification of allochthonous, fluvially-deposited POC as a function of floodplain storage time. We hypothesize that POC oxidation during floodplain storage causes decreased allochthonous POC concentration and ^{13}C-enrichment in the residual allochthonous POC with time spent in floodplain storage. We examine our hypothesis in the Rio Bermejo, Argentina, by comparing bulk POC concentration and carbon isotopic composition of floodplain sediment depth profiles up to 5 m deep across a 20 ky chronosequence to that of actively-transported river sediment. We interpret our data to reflect efficient POC oxidation over millennial timescales, and discuss how feedbacks between climate, tectonics, and Earth surface processes may regulate POC oxidation rates in alluvial basins.

2. Study area and methods

2.1. Study area

We explore POC oxidation across a chronosequence of floodplain deposits of the Rio Bermejo, Argentina ($1.2x10^5$ km^2 drainage area) (Figure 1). The river basin has a subtropical climate with mean annual precipitation and temperature of 1200 mm/y and 22ºC in the headwaters and 700 mm/y and 23ºC in the lowlands, respectively (Harris et al., 2014), and vegetation composed primarily of C_3 shrubs and trees in both the headwaters and lowlands (Figure 1b) (Powell et al., 2012). The headwaters ($5.5x10^4$ km^2) drain the eastern Andes and are underlain by weakly-lithified marine and terrestrial sedimentary rock (McGlue et al., 2016). After exiting the mountain front at ~280 m above sea level, the Bermejo traverses the ~700 km wide Chaco Plain with no tributary inputs except for the Rio Bermejito, a paleochannel of the Bermejo abandoned in an 1870 avulsion (Page, 1889) that contributes <2% and <0.2% of the main stem Rio Bermejo water and sediment discharge, respectively (Orfeo, 2006) (Argentinian National System of Hydrologic Information, https://snih.hidricosargentina.gob.ar/) (Figure 1). Periodic avulsions of the Rio Bermejo have created a fluvial mega-fan (McGlue et al., 2016), extending from the Andean mountain front to the Rio Paraguay. The latter collects the discharge of the Rio Bermejo and conveys it to the Rio Paraná and the Atlantic Ocean.

We limit our analyses to the lowland Rio Bermejo between the confluence of the Rio San Francisco and the river terminus at the Rio Paraguay (Figure 1). The lowland Rio Bermejo is ~4-8 m deep, and has a high suspended sediment load (~3–24 g/L) and relatively fine grain sizes (sand to silt) (Repasch et al., 2020). Recent work using meteoric ^{10}Be suggests a mean transit time of 8.4 ± 2.2 ky for sediment to traverse the lowland Rio Bermejo system (Repasch et al., 2020).

2.2. Sampling strategy and methods

High channel migration rates and periodic avulsions (McGlue et al., 2016; Repasch et al., 2020) create a wide distribution of floodplain deposit ages that we use to build a chronosequence. We compare POC content and isotopic composition in floodplain deposits to sediment in active transport in the Rio Bermejo, which includes both mineral-bound organic carbon and discrete particles of organic detritus. As actively-transported river sediment supplies allochthonous POC to floodplains, this material represents time zero of the floodplain chronosequence (assuming this signal has remained constant throughout the time period of interest).

We collected floodplain deposits and sediment from the active channel over three field campaigns during periods of high flow near the end of the rainy season (May 2015, March 2016, and March 2017). We observed the inundation of channel bars, fresh overbank deposits and lateral channel migration during our sampling, suggesting that the high flows experienced during sampling are characteristic of the flow magnitude during floodplain formation. To account for hydrodynamic sorting during fluvial transport (Galy et al., 2008a; Lupker et al., 2011), we collected bedload and suspended sediment depth profiles at four locations along the Rio Bermejo (Figure 1, Table S1), and supplemented river depth profiles with additional samples of surface water sediment and channel bars exposed as flow receded (Figure 1). To separate liquid and solid phases, we filtered all suspended sediment samples with a 0.22 μm polyethersulfone filter under pressure (Galy and Eglinton, 2011).

We collected 15 floodplain sediment depth profiles from the active channel belt, paleochannels and floodplains using a hand auger (Figure 1 and S1, Table 1). All floodplain coring sites had surface vegetation overlaying an organic-rich soil layer developed in fluvially-deposited sediment (Figure S1). We removed vegetation, leaf litter, and loose, unconsolidated topsoil from sites prior to coring. Profile cores were always above the modern groundwater table, and the groundwater table depth varied between sites from 0.9 m to >5.5 m. We amalgamated individual samples over ~20–40 cm depth increments. Based on sample texture and color, we observed no evidence for paleosols at depth. For select coring sites we collected the top ~2 cm of topsoil as well as leaf litter and organic debris within a ~2 m radius of the auger hole to help distinguish fluvially-deposited allochthonous POC from autochthonous POC produced *in situ* after deposition.

2.3 Sediment physical characterization and geochemistry

In the laboratory, samples were oven dried (>24 h at 40–50 ºC) before homogenization and disaggregation using a mortar and pestle, removal of coarse plant material (>1 mm using tweezers), and splitting into separate aliquots for physical characterization and geochemical analyses.

2.3.1. Sediment grain size distribution, surface area, and Al/Si ratio

POC content often varies with particle size and surface area, with finer, clay-rich sediment typically enriched in POC relative to coarser material (e.g., Bianchi et al., 2018; Galy et al., 2008b). Thus, evaluating the loss of POC with time spent in floodplain storage requires comparing sediment with similar physical characteristics, and we accomplish this by measuring particle size distributions, mineral specific surface area, and Al/Si ratios.

We characterized grain size distributions using a laser diffraction particle-size analyzer (Retsch/Horiba LA950). We pre-treated samples in a sodium pyrophosphate dispersion agent for >24 h to break down aggregates before making 10 replicate measurements of which we report the median value. Repasch et al. (2020) report mineral specific surface area (SSA) on a subset of the samples analyzed here via gas sorption analysis with organic matter removed via combustion prior to measurement (Table S1). We explored the relationship between the fraction of grains finer than a given diameter and SSA. The fraction of grains finer than 2 μm in a sample (f_2) showed the strongest correlation with SSA (R^2 = 0.85, Figure S2), and we use f_2 as a proxy for SSA in our analysis. We additionally measured the Al/Si ratio of select samples using x-ray florescence spectrometry (XRF) as an independent measure of sediment properties. Samples with high Al/Si ratios tend to have high clay content and high POC content relative to samples with low Al/Si ratios (e.g., Galy et al., 2008b). XRF measurements were made by first powdering samples in a disc mill to <63 μm. The powdered samples were heated overnight at 105°C and prepared as fused glass discs with Li-tetraborate-metaborate flux (FLUXANA FX-X65) at a weight ratio of sample to flux of 1:6. After measuring loss on ignition (LOI) in a subsample, the major element oxides (SiO_2, TiO_2, Al_2O_3, Fe_2O_3, MnO, MgO, CaO, Na_2O, K_2O, and P_2O_5) and some trace elements (Ba, Cr, Ga, Nb, Ni, Rb, Sr, Y, Zn, Zr) were analyzed using a PANalytical AXIOS Advanced WDXRF spectrometer equipped with a rhodium anode end-window X-ray tube operated at 2.7 kV. We performed calibration and monitoring of samples and 130 certified international and internal reference samples, which were used for correction procedures.

2.3.2. Sediment organic geochemistry

Aliquots for organic carbon concentration and isotopic analyses were powdered in a disc mill and decarbonated via rinsing in 4% HCl solution following Galy et al. (2007). We made all POC weight percent and isotopic concentration measurements on the remaining solids after discarding and rinsing off the HCl-leach solution. The HCl-leach method we used may lead to greater organic carbon losses than HCl fumigation, and discrepancies may arise when comparing our organic carbon measurements with samples that underwent a different decarbonation method (e.g., Komada et al., 2008). We split POC content and stable carbon isotope ($\delta^{13}C_{org}$) measurements between facilities at the German Research Centre for Geosciences (GFZ) and Durham University. GFZ measurements were made using a NC2500 Carlo Erba elemental analyzer (EA) coupled with a ConFlo III interface on a ThermoFisher Scientific DELTAplusXL isotope ratio mass spectrometer (IRMS), and Durham University measurements used a Costech EA coupled via a ConFlo III to a Thermo Scientific Delta V Advantage IRMS. We performed measurement calibration at GFZ using elemental (Urea) and certified isotope standards (USGS24, IAEA-CH-7) and proofed with an internal soil reference sample (Boden3, HEKATECH). Measurements at Durham University were normalized with internal and international standards and corrected for internal and procedural blanks (e.g., Frith et al., 2018). We measured radiocarbon content of the HCl-leached samples using a combined EA and accelerator mass spectrometer (EA-AMS) system at ETH Zurich (McIntyre et al., 2017; Ruff et al., 2010). We report POC concentration as weight percent organic carbon (using the notation C_{org} to distinguish POC weight percent from POC generically) and stable carbon isotopes using $\delta^{13}C_{org}$ notation in units of permil (‰) relative to Vienna Pee Dee Belemnite (VPDB). We use replicate measurements of C_{org} and $\delta^{13}C_{org}$ to assess uncertainty from both sample heterogeneity and instrument error. We report $^{14}C/^{12}C$ ratios as fraction modern (*Fm*, equivalent to $F^{14}C$ as defined by Reimer et al. (2004)) relative to 95% of the ^{14}C activity of NBS Oxalic Acid II in 1950 ($\delta^{13}C_{org}$ = -17.8‰) and normalized to $\delta^{13}C_{org}$ = -25‰ of VPDB. In the Supplementary Text we describe methods for separating POC_{bio} and POC_{petro}.

2.4 Floodplain depositional ages and aggradation rates

We identified floodplain material deposited after 1984 via historical image analysis in the Google Earth Engine Digitisation Tool (Lea, 2018). For such deposits, we set the minimum deposit age based on the time difference since the Rio Bermejo last occupied the location of the floodplain core. While the maximum age of these deposits is unconstrained, their position in the active Rio Bermejo channel belt (Figure 1), the lack of mature trees (Figure S1), and the shallow coring depth (0.9–2.9 m) relative to Rio Bermejo channel depth (~5 m), are all consistent with a young depositional age relative to our other samples.

To establish a maximum floodplain age for floodplains formed before 1984, we dated deposits using radiocarbon content of charcoal remnants (measured at Poznań Radiocarbon Laboratory, Poland). Deposits lacking charcoal were dated using optically stimulated luminescence (OSL) analyses by Repasch et al. (2020) (Table S2). No deposits had both OSL and charcoal age estimates. For floodplain deposits, we provide a conservative range of formation ages by estimating minimum and maximum ages which account for method-specific measurement uncertainty, measured floodplain aggradation rates based on multiple OSL or charcoal dates in a single core, and the possibility of charcoal inheritance (Frueh and Lancaster, 2014) (Table 1).

Floodplain core depositional ages range from ~1 y to 20 ky (Tables 1 and S2 (Repasch et al., 2020)). In two cores (FP10 and FP14), OSL and charcoal dates were analyzed at core depths more than one meter apart. OSL age differences for FP14 give aggradation rates of 0.3–2 cm/y, while charcoal dates in FP10 are within error, suggesting rapid deposition (Table S2). Two of the floodplain deposits (FP08 and FP09) were not dated by charcoal, OSL, or image analysis. FP09 is a deposit of the Rio Bermejito paleochannel, and we use the time of abandonment (1870) to infer a minimum deposit age of >150 y (Figure 1e). FP08 is within the Rio Bermejo active channel belt and we infer a 33-y minimum deposit age because we observe no significant erosion at that location over the 33 years of historical imagery (1984–2016). A cross-cutting relationship shows FP08 is younger than FP10 (Figure 1g), and we set the maximum FP08 age to 460 y (the mean age estimate for FP10, Table 1).

3. Results

3.1. POC content, POC composition and physical sediment properties

C_{org} values for river sediments in active transport range from 0.02% to 0.5%, and C_{org} tends to be higher for fine-grained sediments with high Al/Si ratios relative to coarse-grained sediments (Figures 2 and S3, Table S1). Fine-grained floodplain sediment with high Al/Si ratios similarly has relatively high C_{org} content, but spans a wider range of C_{org} values (0.01%–5%) than river sediment, likely due to autochthonous POC additions (Figure 2 and S3). Bulk $\delta^{13}C_{org}$

values of actively-transported river sediment range from -27.4‰ to -24.9‰ and finer-grained sediment with higher Al/Si ratios is slightly more enriched in ^{13}C. Floodplain sediment has a substantially wider range of $\delta^{13}C_{org}$ values (-30.2‰ to -14.6‰) than river sediment, and these values show no systematic dependence on grain size or Al/Si ratio (Figures 2 and S3). River suspended sediment has $Fm > 0.8$, similar to other lowland rivers (Galy and Eglinton, 2011; Marwick et al., 2015; Torres et al., 2017), and *Fm* values are greater for suspended sediment with coarser grain sizes and smaller Al/Si ratios. However, bedload and coarse bar material range from $0.59 < Fm < 0.84$, likely reflecting the presence of POC_{petro} (Figures 2, S3, S4 and Supplementary Text). Material from floodplain cores ranges from $0.45 < Fm < 1.07$, also suggesting the presence of POC_{petro} (Supplementary Text). Floodplain samples with high *Fm* values are typically finer-grained sediments with larger Al/Si ratios (Figures 2 and S3) that tend to be near the floodplain surface (Figure 3b and 3d).

3.2. Depth-dependent POC variations in floodplain deposits

Floodplain cores vary in grain size, POC content, and POC isotopic composition as a function of depth (Figures 3, 4 and S5). For deposits older than 150 y, C_{org} generally decreases down core. C_{org} in younger deposits (<30 y) decreases from ~0.5 to 1 m depth, but we find no systematic relationship between C_{org} and core depths greater than ~1 m (Figure 4a and 4c). Variability in C_{org} with depth can be partially attributed to down-core variations in sediment grain size and Al/Si (Figures 2, 3, S3 and S5). In cores where grain size is roughly constant with depth (e.g., FP15), C_{org} decreases almost monotonically down core (Figure 4).

Floodplain core $\delta^{13}C_{org}$ values show no systematic down-core trend (Figure 3a and 3c). However, average $\delta^{13}C_{org}$ values systematically increase with deposit age, displaying a ~9‰ increase from the youngest to oldest deposit (Figure 5a). Top soil and fresh leaf litter samples yield consistently more depleted $\delta^{13}C_{org}$ values than sediment from the co-located core, with the exception of FP09, for which leaf litter is more ^{13}C-enriched than the underlying sediments (Figure 5a, Table S1). The ~5‰ increase in $\delta^{13}C_{org}$ of topsoil and leaf litter across the floodplain chronosequence may be due in part to vegetation differences between sites. Older floodplains tend to be either further away from or elevated above the modern channel relative to younger deposits, and have had more time for ecosystem succession to occur.

All floodplain deposits older than 150 y show a general decrease in *Fm* with increasing core depth, implying a greater relative abundance of either aged POC_{bio} or POC_{petro} moving down core (Figure 3b and 3d). We observe no systematic trend in *Fm* with depth for deposits younger than 150 y, and in some cores we observe $Fm \approx 1$ at 1–1.5 m depth (FP02 and FP08, Figure 3).

4. Testing of allochthonous POC oxidation in floodplain storage

Here we test our hypothesis of ongoing oxidation of POC in floodplains. We first test for a progressive reduction of allochthonous C_{org} with time spent in floodplain storage by separating the contribution of autochthonous versus allochthonous POC in floodplain deposits, and then comparing allochthonous POC concentrations across the chronosequence. As a second test of our hypothesis, we examine how floodplain sediment $\delta^{13}C_{org}$ changes across the chronosequence, under the assumption that isotope fractionation during organic matter decomposition yields residual organic carbon that is ^{13}C-enriched (Natelhoffer and Fry, 1988; Wynn, 2007). Finally, we evaluate the potential for changes in the initial concentration and isotopic composition of allochthonous POC over the chronosequence timescale, as such changes would complicate our interpretation of floodplain oxidation.

4.1. Reduction in allochthonous POC concentration with time spent in floodplain storage

4.1.1 Separating allochthonous and autochthonous POC in floodplain deposits

Actively-transported sediment within the Rio Bermejo is, by definition, purely allochthonous. In contrast, floodplains contain a mix of allochthonous and autochthonous POC, i.e. POC sourced from fluvial deposition, in situ vegetation growth and soil development. To estimate the amount of allochthonous POC lost during floodplain storage, we must first separate the relative contributions of allochthonous and autochthonous POC. We assume two end-member mixing, such that

$$C_{org} = C_{allo} + C_{auto} \text{ (Eq. 1)}$$

and

$$Fm = \frac{C_{auto}}{C_{org}} Fm_{auto} + \frac{C_{allo}}{C_{org}} Fm_{allo} \text{ (Eq. 2).}$$

where C_{auto} and C_{allo} are the weight percentages of the autochthonous and allochthonous POC pools, respectively, and Fm_{auto} and Fm_{allo} are the fraction modern values of the autochthonous and allochthonous POC pools, respectively. For lowland floodplains far from erodible bedrock, such as in the Rio Bermejo, allochthonous POC by definition can include both pre-aged POC_{bio} and POC_{petro}, whereas autochtonous POC is exclusively POC_{bio}, such that we expect $Fm_{auto} \geq Fm \geq Fm_{allo}$. Combining Eq. (1) and (2) and re-arranging yields

$$C_{allo} = C_{org} \frac{(Fm_{auto} - Fm)}{(Fm_{auto} - Fm_{allo})} \text{ (Eq. 3).}$$

Solving for the weight percent of allochthonous POC thus requires knowing Fm and C_{org}, which we directly measured in our samples, and Fm_{auto} and Fm_{allo}, which we estimate below.

As a decrease in allochthonous POC with time spent in floodplain storage is consistent with our hypothesis of ongoing floodplain oxidation, we chose to conservatively estimate total POC oxidation, by setting Fm_{auto} and Fm_{allo} to values that maximize C_{allo} and thus minimize estimates of POC loss. We set Fm_{auto} = 1.07, the highest Fm value measured from all floodplain samples. A high value of Fm_{auto} maximizes the numerator in Eq. (3), thereby maximizing the fraction of allochthonous POC in a sample.

To estimate Fm_{allo}, we account for radiocarbon decay of allochthonous POC since the time of the floodplain formation following

$$Fm_{allo} = Fm_0 e^{(-\lambda t)} \text{ (Eq. 4)},$$

where Fm_0 is the Fm value of allochthonous POC at the time of floodplain deposition, λ is the ^{14}C decay constant (1.209×10^{-4} y^{-1}), and t is the time passed since deposition, in years, which is set to our central age estimates (Table 1). We estimate Fm_0 acknowledging that allochthonous POC is a mix of a pre-aged POC_{bio} and POC_{petro} (e.g., Galy and Eglinton, 2011; Lininger et al., 2019; Torres et al., 2020) (Figures 2 and S4), and therefore should be characterized by an Fm value less than that of the atmosphere at the time of deposition. All of our modern Rio Bermejo river sediment samples have $Fm \leq 0.94$, at least 0.11 lower than the modern Southern Hemisphere atmospheric Fm (1.05). We assume that both fluvial dynamics and organic carbon cycling in the Rio Bermejo have remained constant over the 20-ky chronosequence timespan, such that the >0.11 difference in Fm between the atmosphere and river sediments is constant through time. We thus calculate Fm_0 as

$$Fm_0 = Fm_{atm} - 0.11 \text{ (Eq. 5)}$$

where Fm_{atm} is the atmospheric Fm at the time of floodplain formation (i.e., $F^{14}R_{x\text{-}atm}$=1 following the notation of Soulet et al. (2016)) using the SHCal13 Southern Hemisphere Zone 1-2 reconstruction (Hogg et al., 2013; Hua et al., 2013). This approach maximizes the value of Fm_{allo}, thereby maximizing our estimate of C_{allo} in Eq. (3), and resulting in minimum estimates of allochthonous POC oxidation during floodplain storage. For some samples, the measured Fm

was less than our calculated Fm_{allo} and we set $C_{allo} = C_{org}$ as it is plausible that these cases have no autochthonous POC contribution.

Using the above approach, our over-prediction of C_{allo} relative to the sample's actual value is likely greatest for samples from the oldest floodplain deposits or from deposits containing the coarsest sediment, or both. For floodplain deposits that are hundreds to thousands of years old, our estimate of $Fm_{auto} = 1.07$ is likely too large. In these deposits, a portion of the autochthonous POC has been subject to radiocarbon decay for centuries to millennia, such that Fm_{auto} is likely lower, and if the true value of Fm_{auto} was known, we would calculate a lower weight percent of allochthonous POC. Similarly, samples with coarse sediment tend to have lower *Fm* values than finer sediment (Figures 2 and S3), such that our estimate of Fm_0 in Eq. (5) likely results in an overestimate of Fm_{allo} and C_{allo} for coarse sediment.

Following the above approach yields estimates for the fraction of allochthonous POC in floodplain deposits (C_{allo}/C_{org}) ranging from ~0.004 to 1 (Figure 6). All studied floodplain deposits older than ~10^2 y contain several samples with $C_{allo}/C_{org}<1$, indicating sediment is a mix of autochthonous and allochthonous POC (Figure 6). Samples at shallow depth tend to have lower C_{allo}/C_{org} values, consistent with previous observations (e.g., Hoffmann et al., 2009; Lininger et al., 2018). This may be due to depth-dependent vertical mixing (Gray et al., 2020) of autochthonous POC or percolation of autochthonous dissolved organic carbon (e.g., Kammer and Hagedorn, 2011) produced at the floodplain surface. In the oldest floodplain core (FP15), all samples have $C_{allo}/C_{org}<1$, indicating autochthonous POC up to 5 m depth, and suggesting that autochthonous POC may dominate in Rio Bermejo floodplains over 10^4 y storage timescales.

4.1.2 Progressive reduction in allochthonous POC concentration with floodplain storage time

To test the hypothesis that allochthonous POC is oxidized during floodplain storage, we compare POC concentration across the floodplain chronosequence against actively-transported river sediment. Assuming constant POC loading through time, a progressive decrease in POC concentration from actively-transported river sediment to aged floodplain deposits indicates ongoing allochthonous POC oxidation. We test this for bulk C_{org}, which includes both autochthonous and allochthonous POC, and for our conservative estimate of C_{allo}. We account for the correlation of organic carbon with fine, Al-rich sediment (Figures 2 and S3) by comparing POC concentration in samples with similar grain size distributions and Al/Si ratios. This assumes that the grain size distribution and Al/Si ratio of floodplain sediments did not significantly change over the ~20-ky of our chronosequence. Such an assumption seems justified, as the oldest floodplain deposit (FP15, which we interpret to be a point bar deposit) has grain size distributions and Al/Si ratios approximately equal to the coarse bedload we collected from the modern Rio Bermejo (Figures 2, 7, S3, and S6).

POC concentrations progressively decrease with time spent in floodplain storage (Figure 7). C_{org} of floodplain sediment, including both autochthonous and allochthonous contributions, from deposits older than ~10^3 y and deeper than ~2 m is consistently ~50–80% lower than that of actively-transported river sediment and recently deposited floodplain sediment (<~50 y) with similar grain size distributions. This difference increases up to an order of magnitude when comparing actively-transported river sediment to allochthonous POC in the oldest floodplain deposit (Figure 7). Deep (>2 m) sediment from floodplain deposits with depositional ages of ~10^2 y have C_{org} values both equal to and lower than actively-transported river sediment, while deep samples from deposits younger than ~10^2 y tend to have C_{org} values approximately equal to those observed in actively-transported river sediment (Figure 7). Shallow floodplain samples (<1 m depth) generally have C_{org} values approximately equal to or higher than actively-transported river sediment, independent of floodplain age (Figure 7), in part due to larger contributions of autochthonous POC (Figure 6). C_{allo} of deposits older than ~10^3 y tends to be lower than C_{org} of actively-transported river sediments across all depths (Figure 7).

We interpret these results to suggest that significant oxidation of allochthonous POC in floodplains requires millennial timescales (Figure 7). The measured 50–80% loss of C_{org} and up to order of magnitude loss of C_{allo} between modern river and 10^3 y old floodplain sediment of similar grain size likely under-estimate the true extent of allochthonous POC oxidation, due to our conservative approach in estimating C_{allo}. Furthermore, the agreement in allochthonous POC oxidation between the two oldest cores (FP14 and FP15, which plot as yellow and orange symbols in Figure 7), limits the possibility that these observations are due to random chance. Repeating this analysis using the Al/Si ratio or median grain diameter of samples as a metric of grain size yields broadly consistent results (Figure S6). However, in these cases, the loss of POC in the oldest floodplain core (FP15) is not as evident as when using f_2 as a metric of particle size distribution. For FP15, the bulk C_{org} (including allochthonous and autochthonous POC) in floodplain samples is generally equal to or greater than the C_{org} of actively transported river sediments with similar Al/Si ratios or median grain diameter. However, the allochthonous POC weight percent of deep floodplain samples can be up to ~30% lower than actively-transported river sediment, consistent with our hypothesis of oxidation of allochthonous POC in floodplain storage. The variability of FP15 among our analyses with f_2, median grain size, and Al/Si ratio stems from a slightly bimodal grain size distribution for samples in this deposit (Figure S7). The f_2 metric captures the presence of a small fraction of fine material in this sample that is not reflected in the median grain size or Al/Si ratio, but may hold a large portion of POC given the association between POC and fine sediment (e.g., Bianchi et al., 2018). Furthermore, FP15 is the oldest deposit and has the coarsest sediment, such that we are almost certainly over-estimating the amount of allochthonous POC present in the deposit, and therefore underestimating the total amount of allochthonous POC oxidation since the time of deposition.

4.2 Enrichment in $\delta^{13}C_{org}$ with time

Oxidation of allochthonous POC during floodplain storage may also be recorded by changes in the POC stable carbon isotope composition. ^{13}C-enrichment of soil organic carbon with time is well documented. While the mechanism of ^{13}C-enrichment is debated (e.g., Ehleringer et al., 2000), isotopic fractionation of POC during oxidation is one proposed cause (e.g., Wynn, 2007). Under this scenario, preferential removal of ^{12}C during decomposition would leave behind POC that is ^{13}C-enriched. Other mechanisms for ^{13}C-enrichment of POC include, but are not limited to, input of autochthonous POC from C_4 vegetation (e.g., Lininger et al., 2018), microbial processing of existing POC (e.g., Dijkstra et al., 2006), dissolved organic carbon eluviation from overlying leaf litter and soils (e.g., Kammer and Hagedorn, 2011), and production of microbial and fungal residues (e.g., Ehleringer et al., 2000). All of these mechanisms would lead to progressive ^{13}C-enrichment in residual autochthonous and allochthonous POC within floodplain deposits.

We observe a ~9‰ increase in $\delta^{13}C_{org}$ between actively-transported river sediment and the oldest floodplain deposit (Figure 5). Both leaf litter and topsoil appear more ^{13}C-enriched at the locations of the oldest floodplain deposits (Figure 5a); we account for this by calculating the difference in $\delta^{13}C_{org}$ between each floodplain sediment sample and its overlying modern leaf litter. Comparing these differences across the chronosequence shows a ~5‰ increase in $\delta^{13}C_{org}$ from the youngest to the oldest floodplain deposit (Figure 5b). While we cannot distinguish between the proposed mechanisms for ^{13}C-enrichment, we argue that the observed ^{13}C-enrichment is consistent with oxidation of both allochthonous and autochtonous POC during floodplain storage.

4.3. Evaluation of temporally constant C_{org} and $\delta^{13}C_{org}$ input

Our floodplain chronosequence data show that increasing time in floodplain storage results in reduced allochthonous POC in floodplain deposits and elevated floodplain $\delta^{13}C_{org}$ values. While these observations are consistent with decomposition of allochthonous POC in floodplain storage, such trends could emerge in the absence of POC oxidation if river sediment experienced a systematic increase in C_{org} and a decrease in $\delta^{13}C_{org}$ over the ~20-ky period covered by our chronosequence.

We argue it is unlikely that C_{org} of river sediment systematically increased over the past 20 ky in the Rio Bermejo. While we lack paleoclimate data from the Rio Paraná delta (the sink of Rio Bermejo sediment) which could most directly test this hypothesis, off the coast of Brazil organic carbon accumulation rates were generally higher from 19–23 ka relative to 4–8 ka (Mollenhauer et al., 2004). This is supported by biomarker data suggesting large pulses of terrigenous organic matter were common from 18–28 ka (Lourenco et al., 2016). Furthermore, the C_{org} and C_{allo} values from deep (>2 m depth) sediment of the two oldest floodplain deposits in our chronosequence (FP14, 2–4 ky, and FP15, 1.2–20.2 ky) have C_{org} <0.1%. These C_{org} values are low relative to the typically >0.1% modern C_{org} values measured in sediment in rivers and coastal environments spanning a range of grain sizes and climatic environments (Bianchi et al., 2018; Hilton, 2017; Marwick et al., 2015), such that it seems unlikely these low levels were sustained over the millennial timespan of our chronosequence.

Evaluating if there was a systematic shift in the $\delta^{13}C_{org}$ value of allochthonous POC over the past 20 ky is more difficult. A shift in vegetation from C_4-dominated plants (which tend to be ^{13}C-enriched) to C_3-dominated vegetation (which tends to be ^{13}C-depleted) could yield a trend of increasing $\delta^{13}C_{org}$ with depositional age, similar to that observed in our floodplain deposits. Others have argued for such a shift in central Argentina based on $\delta^{13}C_{org}$ values of soil and floodplain cores from <1 m depth (Silva et al., 2011). This approach is problematic, as it ignores both the possibility for changes in carbon isotope composition during storage which could produce such trends (e.g., Ehleringer et al., 2000; Wynn, 2007), and the possibility of overprinting allochthonous POC at shallow depth by recently-produced autochthonous POC (Lininger et al., 2018; Zehetner et al., 2009). A more robust test of a shift in vegetation could come from compound-specific ^{13}C measurements (e.g., Garcin et al., 2014), and such measurements should be a target for future work. While we cannot fully rule out the possibility that POC loading and stable carbon isotope composition has varied with time, we argue that oxidation of allochthonous POC during floodplain storage is the simplest mechanism to fully explain our observed losses in C_{allo} and increases in $\delta^{13}C_{org}$ with time.

5. Implications for geomorphic, tectonic, and climatic controls on POC oxidation

Our observations in the Rio Bermejo floodplain suggest allochthonous POC buried at shallow depth (<5 m) in aerated floodplains can be efficiently incinerated over millennial timescales. Given the shallow river depth (~5 m), we expect the vast majority of POC deposited via channel migration, overbank flow, and periodic avulsions across the Rio Bermejo mega-fan to be subject to oxidation. Furthermore, the ~8.4 ky mean residence time for sediment transiting the lowland Rio Bermejo (Repasch et al., 2020) suggests POC produced in the headwaters is likely to be oxidized during lowland river transit, such that POC exported from the Rio Bermejo is likely to be biased towards organic matter produced in the most downstream portions of the basins (e.g., Hemingway et al., 2017; Torres et al., 2017).

Combining our findings with previous results showing stabilization of POC deposited under anoxic conditions (Boye et al., 2017) implies that oxidation of allochthonous POC in floodplains is set by a balance between storage time and the level of the groundwater table, with potential for complex feedbacks following perturbations in geomorphic, climatic, tectonic and anthropogenic forcing. For example, increases in tectonic uplift rate or transitions to wetter climates can increase sediment supply, causing rivers to aggrade and avulse more frequently (Jerolmack and Mohrig, 2007), while also driving an increase in lateral channel migration rates (Constantine et al., 2014). This aggradation may preserve POC by raising the groundwater table and creating anoxic conditions in floodplains (Boye et al., 2017). Concurrently, increased channel migration rates can reduce the residence time of floodplain-stored material (e.g., Bradley and Tucker, 2013; Repasch et al., 2020; Torres et al., 2017), and thereby limit the time available for POC oxidation if migration is confined within a narrow corridor as is common in lowland migrating rivers (Bradley and Tucker, 2013). Future field, lab, and theoretical efforts to constrain sediment residence time in aerated floodplains under changing climatic and tectonic forcing will be key to deciphering how Earth surface processes regulate terrestrial organic carbon cycling.

Acknowledgements

Support for this work came from an Alexander von Humboldt Postdoctoral Fellowship to J.S.S., Helmholtz Association funding to N. Hovius, the StRATEGy international research training group funded by the German Research Foundation (DFG) and the State of Brandenburg to D.S. and M.R., and the Swiss National Science Foundation (SNF) Grant No. 200020_163162 (CAPS-LOCK2) to T.I.E.. We thank Jordon Hemingway and two anonymous reviewers for constructive feedback and benefited from discussions with M. Dellinger, R. Hilton, and M. Torres. K. Cook, H. Hassenruck-Gudipati, R. Teodoro Casimiro, and H. Wittmann provided field assistance. Sediment grain size analyses were made in the GFZ Sed Lab, and we thank B. Plessen, S. Pinkerneil, and P. Meier for assistance with bulk carbon concentration and stable isotope measurements at GFZ.

Figures Captions:

Figure 1: (a) Digital elevation model of the Rio Bermejo watershed and sampling locations, inset shows study location in northern Argentina. (b) Percent of vegetation made up by C_3 plants from Powell et al. (2012). (c - g) Optical imagery of sampling locations ~200-300 km (c and d) and ~450–500 km (e and f) downstream from the Rio San Francisco junction. Floodplains are labeled from youngest (FP01) to oldest (FP15). Imagery accessed via Google Earth and ESRI ArcMap.

Figure 2: (a and b) Particulate organic carbon weight percent (C_{org}), (c and d) stable carbon isotopes ($\delta^{13}C_{org}$), and (e and f) radiocarbon fraction modern (*Fm*) versus fraction of grains < 2 μm (f_2) for actively-transported suspended and bedload sediment collected in the Rio Bermejo (a, c, and e) and floodplain deposits (b, d, and f). In panels (a, c, and e), color and symbol groupings indicate distance downstream from the junction with the Rio San Francisco (Figure 1), while in (b, d, and f) color and symbol show floodplain depositional age. Error bars show standard deviation from replicate measurements and are smaller than the symbol size where not shown.

Figure 3: Floodplain depth profiles of $\delta^{13}C_{org}$ and radiocarbon fraction modern (*Fm*). (a and b) Show all profiles of $\delta^{13}C_{org}$ and *Fm*, respectively, on the same plot, color-coded by floodplain age. (c and d) Highlight individual profiles of $\delta^{13}C_{org}$ and *Fm*, respectively, for each floodplain core (black line) with profiles from other floodplain cores in gray. Axis extent of individual profiles in (c) and (d) match extent shown in (a) and (b), respectively. Error bars are removed for clarity but are reported in Table S1. Box and whisker plots in (a) and (b) show median, inter-quartile range, and full extent of values observed in actively transported river sediments.

Figure 4: Floodplain depth profiles of POC weight percent (C_{org}) and fraction of grains less than 2 μm (f_2). (a and b) Show all profiles of C_{org} and f_2, respectively, on the same plot, color-coded by floodplain age. (c and d) Highlight individual profiles of C_{org} and f_2, respectively, for each floodplain core (black line) with profiles from other floodplain cores in gray. Axis extent of individual profiles in (c) and (d) match extent shown in (a) and (b), respectively. Error bars are removed for clarity but are reported in Table S1. Box and whisker plots in (a) and (b) show median, inter-quartile range, and full extent of values observed in actively transported river sediments.

Figure 5: (a) Stable carbon isotope values of bulk POC ($\delta^{13}C_{org}$) from floodplain cores, top soil, and leaf litter versus independently constrained floodplain deposit age. Also shown are the $\delta^{13}C_{org}$ range of actively transported fluvial sediment in the Rio Bermejo. (b) Difference between leaf litter and floodplain sample $\delta^{13}C_{org}$. In both panels, floodplain samples are color-coded by depth below surface; white squares show concentration-weighted mean POC values with error bars indicating range in deposit age estimate. Error bars are smaller than the symbol where not shown. Right pointing arrow indicates unconstrained maximum depositional age of FP09.

Figure 6: (a) Radiocarbon fraction modern (*Fm*) and (b) fraction of allochthonous POC (C_{allo}/C_{org}) in floodplain deposits as a function of independently-constrained floodplain depositional age. Symbols are color-coded by sample depth below the floodplain surface, with white squares in (a) showing POC concentration-weighted mean values for the entire floodplain

core with error bars indicating the range in deposit age estimate (smaller than the symbol where not shown). Black line in (a) shows maximum possible *Fm* value for allochthonous POC (Fm_{allo}). Also shown in (a) is range of *Fm* values of river sediment (blue circles are individual samples and white circle is mean of all samples).

Figure 7: Comparison of POC weight percent (C_{org}) versus fraction of grains < 2 μm (f_2) for actively transported river sediment (gray circles) and floodplain deposits (squares and asterisks). Floodplains deposits are color-coded by depositional age and symbol size indicates sample depth below surface. Solid squares show measured C_{org}, asterisks and open squares show calculated allocthonous POC (C_{allo}) in floodplain samples assuming no pre-aged POC or POC_{petro} and permitting pre-aged POC and POC_{petro}, respectively, see text for details. Error bars show standard deviation from replicate measurements, and are smaller than the symbol size when not shown. Floodplain deposit FP09 is ommitted from the figure as we have only a minimum a constraint (150 y) on its age.

References

Aufdenkampe, A.K., Mayorga, E., Hedges, J.I., Llerena, C., Quay, P.D., Gudeman, J., Krusche, A.V., Richey, J.E., 2007. Organic matter in the Peruvian headwaters of the Amazon: Compositional evolution from the Andes to the lowland Amazon mainstem. Organic Geochemistry 38, 337-364.

Baisden, W.T., Amundson, R., Brenner, D.L., Cook, A.C., Kendall, C., Harden, J.W., 2002. A multiisotope C and N modeling analysis of soil organic matter turnover and transport as a function of soil depth in a California annual grassland soil chronosequence. Global Biogeochemical Cycles 16.

Bianchi, T.S., Cui, X., Blair, N.E., Burdige, D.J., Eglinton, T.I., Galy, V., 2018. Centers of organic carbon burial and oxidation at the land-ocean interface. Organic Geochemistry 115, 138-155.

Bouchez, J., Beyssac, O., Galy, V., Gaillardet, J., France-Lanord, C., Maurice, L., Moreira-Turcq, P., 2010. Oxidation of petrogenic organic carbon in the Amazon floodplain as a source of atmospheric CO2. Geology 38, 255-258.

Boye, K., Noël, V., Tfaily, M.M., Bone, S.E., Williams, K.H., Bargar, John R., Fendorf, S., 2017. Thermodynamically controlled preservation of organic carbon in floodplains. Nature Geoscience 10, 415-419.

Bradley, D.N., Tucker, G.E., 2013. The storage time, age, and erosion hazard of laterally accreted sediment on the floodplain of a simulated meandering river. Journal of Geophysical Research-Earth Surface 118, 1308-1319.

Cierjacks, A., Kleinschmit, B., Babinsky, M., Kleinschroth, F., Markert, A., Menzel, M., Ziechmann, U., Schiller, T., Graf, M., Lang, F., 2010. Carbon stocks of soil and vegetation on Danubian floodplains. J Plant Nutr Soil Sc 173, 644-653.

Constantine, J.A., Dunne, T., Ahmed, J., Legleiter, C., Lazarus, E.D., 2014. Sediment supply as a driver of river meandering and floodplain evolution in the Amazon Basin. Nature Geoscience 7, 899-903.

Dijkstra, P., Ishizu, A., Doucett, R., Hart, S.C., Schwartz, E., Menyailo, O.V., Hungate, B.A., 2006. C-13 and N-15 natural abundance of the soil microbial biomass. Soil Biol Biochem 38, 3257-3266.

Ehleringer, J.R., Buchmann, N., Flanagan, L.B., 2000. Carbon isotope ratios in belowground carbon cycle processes. Ecological Applications 10, 412-422.

Frith, N.V., Hilton, R.G., Howarth, J.D., Gröcke, D.R., Fitzsimons, S.J., Croissant, T., Wang, J., McClymont, E.L., Dahl, J., Densmore, A.L., 2018. Carbon export from mountain forests enhanced by earthquake-triggered landslides over millennia. Nature Geoscience 11, 772-+.

Frueh, W.T., Lancaster, S.T., 2014. Correction of deposit ages for inherited ages of charcoal: implications for sediment dynamics inferred from random sampling of deposits on headwater valley floors. Quaternary Sci Rev 88, 110-124.

Galy, V., Beyssac, O., France-Lanord, C., Eglinton, T., 2008a. Recycling of Graphite During Himalayan Erosion: A Geological Stabilization of Carbon in the Crust. Science 322, 943-945.

Galy, V., Bouchez, J., France-Lanord, C., 2007. Determination of total organic carbon content and delta C-13 in carbonate-rich detrital sediments. Geostand Geoanal Res 31, 199-207.

Galy, V., Eglinton, T., 2011. Protracted storage of biospheric carbon in the Ganges-Brahmaputra basin. Nature Geoscience 4, 843-847.

Galy, V., France-Lanord, C., Lartiges, B., 2008b. Loading and fate of particulate organic carbon from the Himalaya to the Ganga-Brahmaputra delta. Geochimica Et Cosmochimica Acta 72, 1767-1787.

Garcin, Y., Schefuss, E., Schwab, V.F., Garreta, V., Gleixner, G., Vincens, A., Todou, G., Sene, O., Onana, J.M., Achoundong, G., Sachse, D., 2014. Reconstructing C-3 and C-4 vegetation cover using n-alkane carbon isotope ratios in recent lake sediments from Cameroon, Western Central Africa. Geochimica Et Cosmochimica Acta 142, 482-500.

Goñi, M.A., Moore, E., Kurtz, A., Portier, E., Alleau, Y., Merrell, D., 2014. Organic matter compositions and loadings in soils and sediments along the Fly River, Papua New Guinea. Geochimica Et Cosmochimica Acta 140, 275-296.

Gray, H.J., Keen-Zebert, A., Furbish, D.J., Tucker, G.E., Mahan, S.A., 2020. Depth-dependent soil mixing persists across climate zones. Proceedings of the National Academy of Sciences of the United States of America 117, 8750-8756.

Harris, I., Jones, P.D., Osborn, T.J., Lister, D.H., 2014. Updated high-resolution grids of monthly climatic observations - the CRU TS3.10 Dataset. Int J Climatol 34, 623-642.

Hemingway, J.D., Hilton, R.G., Hovius, N., Eglinton, T.I., Haghipour, N., Wacker, L., Chen, M.C., Galy, V.V., 2018. Microbial oxidation of lithospheric organic carbon in rapidly eroding tropical mountain soils. Science 360, 209-+.

Hemingway, J.D., Rothman, D.H., Grant, K.E., Rosengard, S.Z., Eglinton, T.I., Derry, L.A., Galy, V.V., 2019. Mineral protection regulates long-term global preservation of natural organic carbon. Nature 570, 228-+.

Hemingway, J.D., Schefuss, E., Spencer, R.G.M., Dinga, B.J., Eglinton, T.I., McIntyre, C., Galy, V.V., 2017. Hydrologic controls on seasonal and inter-annual variability of Congo River particulate organic matter source and reservoir age. Chem Geol 466, 454-465.

Hilton, R.G., 2017. Climate regulates the erosional carbon export from the terrestrial biosphere. Geomorphology 277, 118-132.

Hilton, R.G., West, A.J., 2020. Mountains, erosion and the carbon cycle. Nature Reviews Earth and Environment 1, 284-299.

Hoffmann, T., Glatzel, S., Dikau, R., 2009. A carbon storage perspective on alluvial sediment storage in the Rhine catchment. Geomorphology 108, 127-137.

Hogg, A.G., Hua, Q., Blackwell, P.G., Niu, M., Buck, C.E., Guilderson, T.P., Heaton, T.J., Palmer, J.G., Reimer, P.J., Reimer, R.W., Turney, C.S.M., Zimmerman, S.R.H., 2013. Shcal13 Southern Hemisphere Calibration, 0-50,000 Years Cal Bp. Radiocarbon 55, 1889-1903.

Hua, Q., Barbetti, M., Rakowski, A.Z., 2013. Atmospheric Radiocarbon for the Period 1950-2010. Radiocarbon 55, 2059-2072.

Jerolmack, D.J., Mohrig, D., 2007. Conditions for branching in depositional rivers. Geology 35, 463-466.

Kammer, A., Hagedorn, F., 2011. Mineralisation, leaching and stabilisation of C-13-labelled leaf and twig litter in a beech forest soil. Biogeosciences 8, 2195-2208.

Komada, T., Anderson, M.R., Dorfmeier, C.L., 2008. Carbonate removal from coastal sediments for the determination of organic carbon and its isotopic signatures, delta C-13 and Delta C-14: comparison of fumigation and direct acidification by hydrochloric acid. Limnol Oceanogr-Meth 6, 254-262.

Lawrence, C.R., Harden, J.W., Xu, X.M., Schulz, M.S., Trumbore, S.E., 2015. Long-term controls on soil organic carbon with depth and time: A case study from the Cowlitz River Chronosequence, WA USA. Geoderma 247, 73-87.

Lea, J.M., 2018. The Google Earth Engine Digitisation Tool (GEEDiT) and the Margin change Quantification Tool (MaQiT) - simple tools for the rapid mapping and quantification of changing Earth surface margins. Earth Surf Dynam 6, 551-561.

Lininger, K.B., Wohl, E., Rose, J.R., 2018. Geomorphic Controls on Floodplain Soil Organic Carbon in the Yukon Flats, Interior Alaska, From Reach to River Basin Scales. Water Resources Research 54, 1934-1951.

Lininger, K.B., Wohl, E., Rose, J.R., Leisz, S.J., 2019. Significant Floodplain Soil Organic Carbon Storage Along a Large High-Latitude River and its Tributaries. Geophysical Research Letters 46, 2121-2129.

Lourenco, R.A., de Mahiques, M.M., Wainer, I.E.K.C., Rosell-Mele, A., Bicego, M.C., 2016. Organic biomarker records spanning the last 34,800 years from the southeastern Brazilian upper slope: links between sea surface temperature, displacement of the Brazil Current, and marine productivity. Geo-Mar Lett 36, 361-369.

Lupker, M., France-Lanord, C., Lave, J., Bouchez, J., Galy, V., Metivier, F., Gaillardet, J., Lartiges, B., Mugnier, J.L., 2011. A Rouse-based method to integrate the chemical composition of river sediments: Application to the Ganga basin. Journal of Geophysical Research-Earth Surface 116, 24.

Marwick, T.R., Tamooh, F., Teodoru, C.R., Borges, A.V., Darchambeau, F., Bouillon, S., 2015. The age of river-transported carbon: A global perspective. Global Biogeochemical Cycles 29, 122-137.

Masiello, C.A., Chadwick, O.A., Southon, J., Torn, M.S., Harden, J.W., 2004. Weathering controls on mechanisms of carbon storage in grassland soils. Global Biogeochemical Cycles 18.

McGlue, M.M., Smith, P.H., Zani, H., Silva, A., Carrapa, B., Cohen, A.S., Pepper, M.B., 2016. An Integrated Sedimentary Systems Analysis of the Rio Bermejo (Argentina): Megafan Character in the Overfilled Southern Chaco Foreland Basin. Journal of Sedimentary Research 86, 1359-1377.

McIntyre, C.P., Wacker, L., Haghipour, N., Blattmann, T.M., Fahrni, S., Usman, M., Eglinton, T.I., Synal, H.A., 2017. Online C-13 and C-14 Gas Measurements by EA-IRMS-AMS at ETH Zurich. Radiocarbon 59, 893-903.

Mollenhauer, G., Schneider, R.R., Jennerjahn, T., Muller, P.J., Wefer, G., 2004. Organic carbon accumulation in the South Atlantic Ocean: its modem, mid-Holocene and last glacial distribution. Global Planet Change 40, 249-266.

Natelhoffer, K.J., Fry, B., 1988. Controls on Natural Nitrogen-15 and Carbon-13 Abundances in Forest Soil Organic Matter. Soil Science Society of America Journal Abstract 52, 1633-1640.

Orfeo, O., 2006. Dynamics of sediment transport in two subtropical plain rivers of South America. Zeitschrift für Geomorphologie 145, 229-241.

Page, J., 1889. The Gran Chaco and its Rivers. Proceedings of the Royal Geographical Society and Monthly Record of Geography 11, 129-152.

Powell, R.L., Yoo, E.H., Still, C.J., 2012. Vegetation and soil carbon-13 isoscapes for South America: integrating remote sensing and ecosystem isotope measurements. Ecosphere 3.

Reimer, P.J., Brown, T.A., Reimer, R.W., 2004. Discussion: Reporting and calibration of post-bomb C-14 data. Radiocarbon 46, 1299-1304.

Repasch, M., Wittmann, H., Scheingross, J.S., Sachse, D., Szupiany, R., Orfeo, O., Fuchs, M., Hovius, N., 2020. Sediment transit time and floodplain storage dynamics in alluvial rivers revealed by meteoric 10Be. J. Geophys. Res. Earth Surf.

Ruff, M., Fahrni, S., Gaggeler, H.W., Hajdas, I., Suter, M., Synal, H.A., Szidat, S., Wacker, L., 2010. On-Line Radiocarbon Measurements of Small Samples Using Elemental Analyzer and Micadas Gas Ion Source. Radiocarbon 52, 1645-1656.

Scheingross, J.S., Hovius, N., Dellinger, M., Hilton, R.G., Repasch, M., Sachse, D., Gröcke, D.R., Vieth-Hillebrand, A., Turowski, J.M., 2019. Preservation of organic carbon during active fluvial transport and particle abrasion. Geology 47.

Schlesinger, W.H., 1990. Evidence from Chronosequence Studies for a Low Carbon-Storage Potential of Soils. Nature 348, 232-234.

Silva, L.C.R., Giorgis, M.A., Anand, M., Enrico, L., Perez-Harguindeguy, N., Falczuk, V., Tieszen, L.L., Cabido, M., 2011. Evidence of shift in C-4 species range in central Argentina during the late Holocene. Plant Soil 349, 261-279.

Soulet, G., Skinner, L.C., Beaupre, S.R., Galy, V., 2016. A Note on Reporting of Reservoir C-14 Disequilibria and Age Offsets. Radiocarbon 58, 205-211.

Torres, M.A., Kemeny, P.C., Lamb, M.P., Cole, T.L., Fischer, W.W., 2020. Long-Term Storage and Age-Biased Export of Fluvial Organic Carbon: Field Evidence From West Iceland. Geochemistry Geophysics Geosystems 21.

Torres, M.A., Limaye, A.B., Ganti, V., Lamb, M.P., West, A.J., Fischer, W.W., 2017. Model predictions of long-lived storage of organic carbon in river deposits. Earth Surf Dynam 5, 711-730.

Wynn, J.G., 2007. Carbon isotope fractionation during decomposition of organic matter in soils and paleosols: Implications for paleoecological interpretations of paleosols. Palaeogeogr Palaeocl 251, 437-448.

Zehetner, F., Lair, G.J., Gerzabek, M.H., 2009. Rapid carbon accretion and organic matter pool stabilization in riverine floodplain soils. Global Biogeochemical Cycles 23.

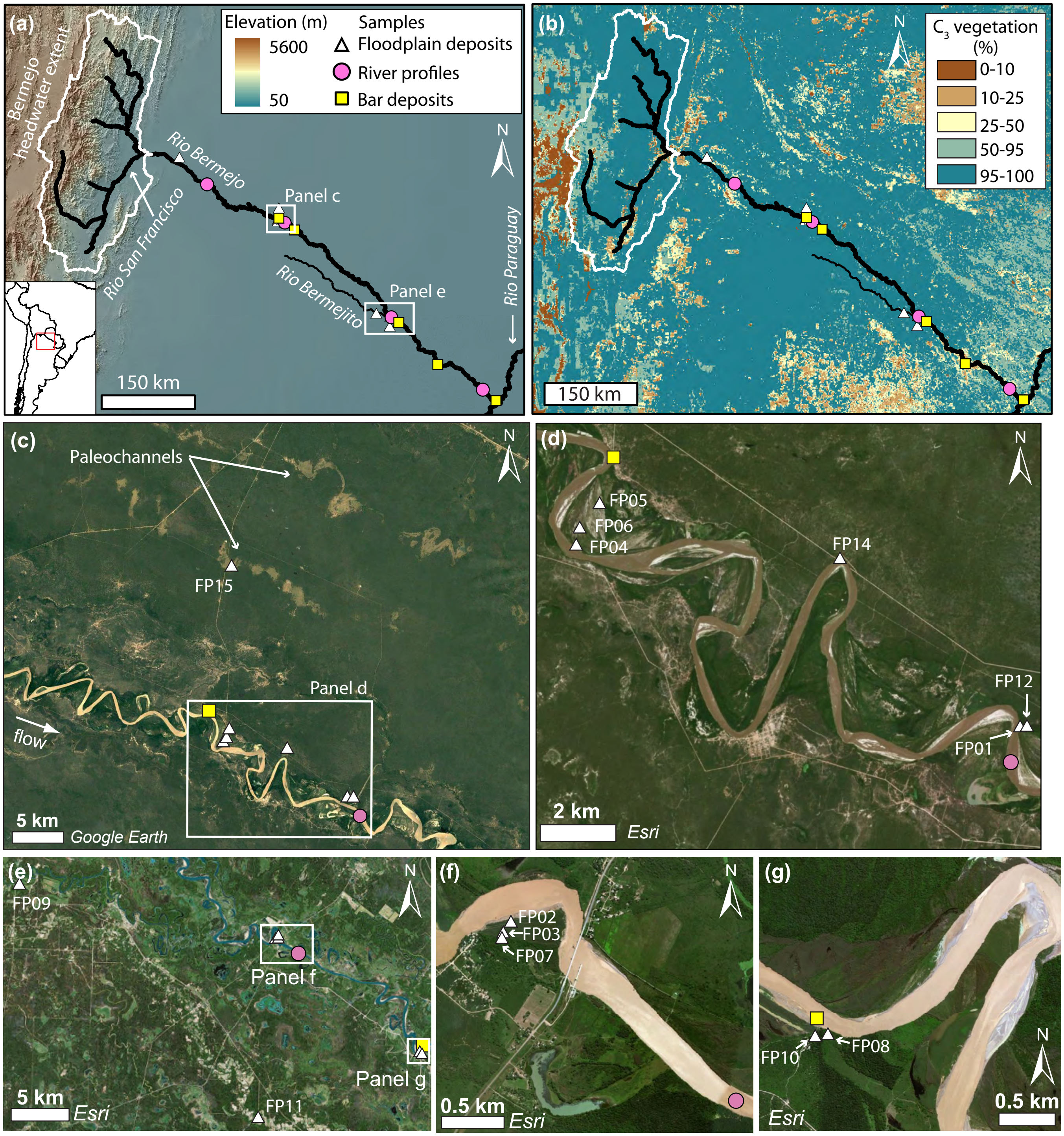

Figure 1: (a) Digital elevation model of the Rio Bermejo watershed and sampling locations, inset shows study location in northern Argentina. (b) Percent of vegetation made up by C_3 plants from Powell et al. [2012]. (c - g) Optical imagery of sampling locations ~200-300 km (c and d) and ~450-500 km (e and f) downstream from the Rio San Francisco junction. Floodplains are labeled from youngest (FP01) to oldest (FP15). Imagery accessed via Google Earth and Esri ArcMap.

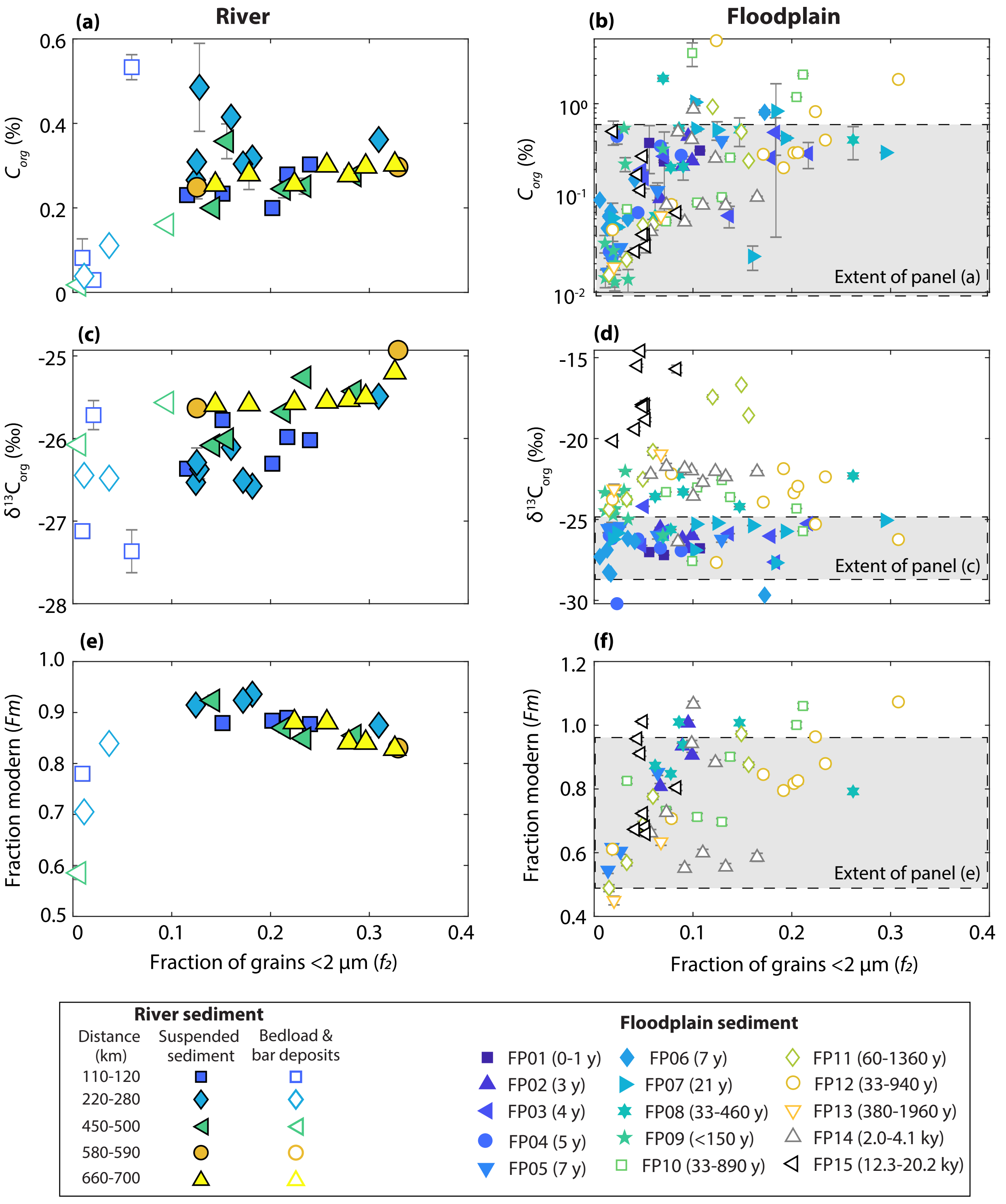

Figure 2: (a and b) Particulate organic carbon weight percent (C_{org}), (c and d) stable carbon isotopes ($\delta^{13}C_{org}$), and (e and f) radiocarbon fraction modern (*Fm*) versus fraction of grains < 2 µm (f_2) for actively-transported suspended and bedload sediment collected in the Rio Bermejo (a, c, and e) and floodplain deposits (b, d, and f). In panels (a, c, and e), color and symbol groupings indicate distance downstream from the junction with the Rio San Francisco (Figure 1), while in (b, d, and f) color and symbol show floodplain depositional age. Error bars show standard deviation from replicate measurements and are smaller than the symbol size where not shown.

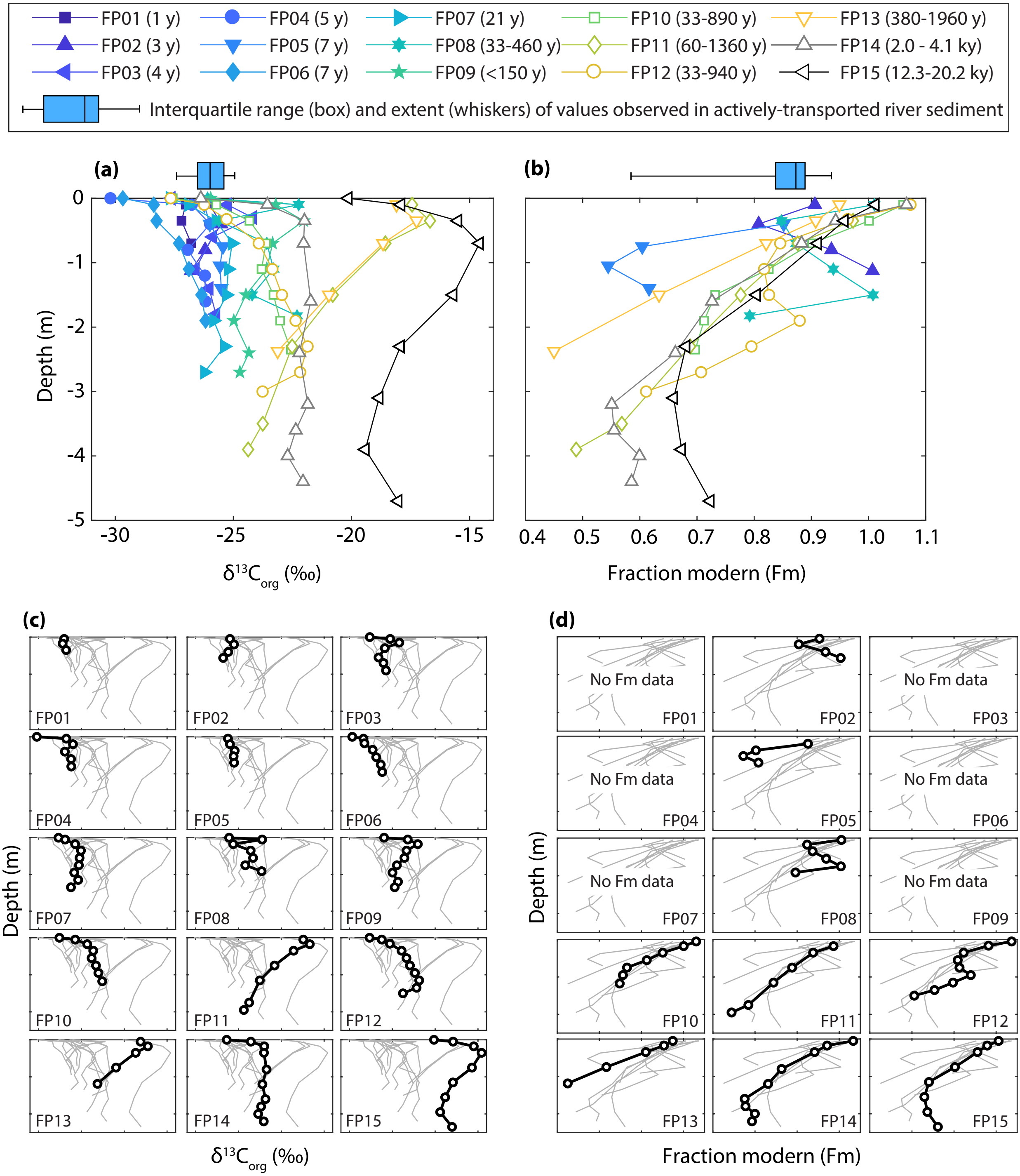

Figure 3: Floodplain depth profiles of $\delta^{13}C_{org}$ and radiocarbon fraction modern (*Fm*). (a and b) Show all profiles of $\delta^{13}C_{org}$ and *Fm*, respectively, on the same plot, color-coded by floodplain age. (c and d) Highlight individual profiles of $\delta^{13}C_{org}$ and *Fm*, respectively, for each floodplain core (black line) with profiles from other floodplain cores in gray. Axis extent of individual profiles in (c) and (d) match extent shown in (a) and (b), respectively. Error bars are removed for clarity, but are reported in Table S1. Box and whisker plots in (a) and (b) show median, inter-quartile range, and full extent of values observed in actively transported river sediments.

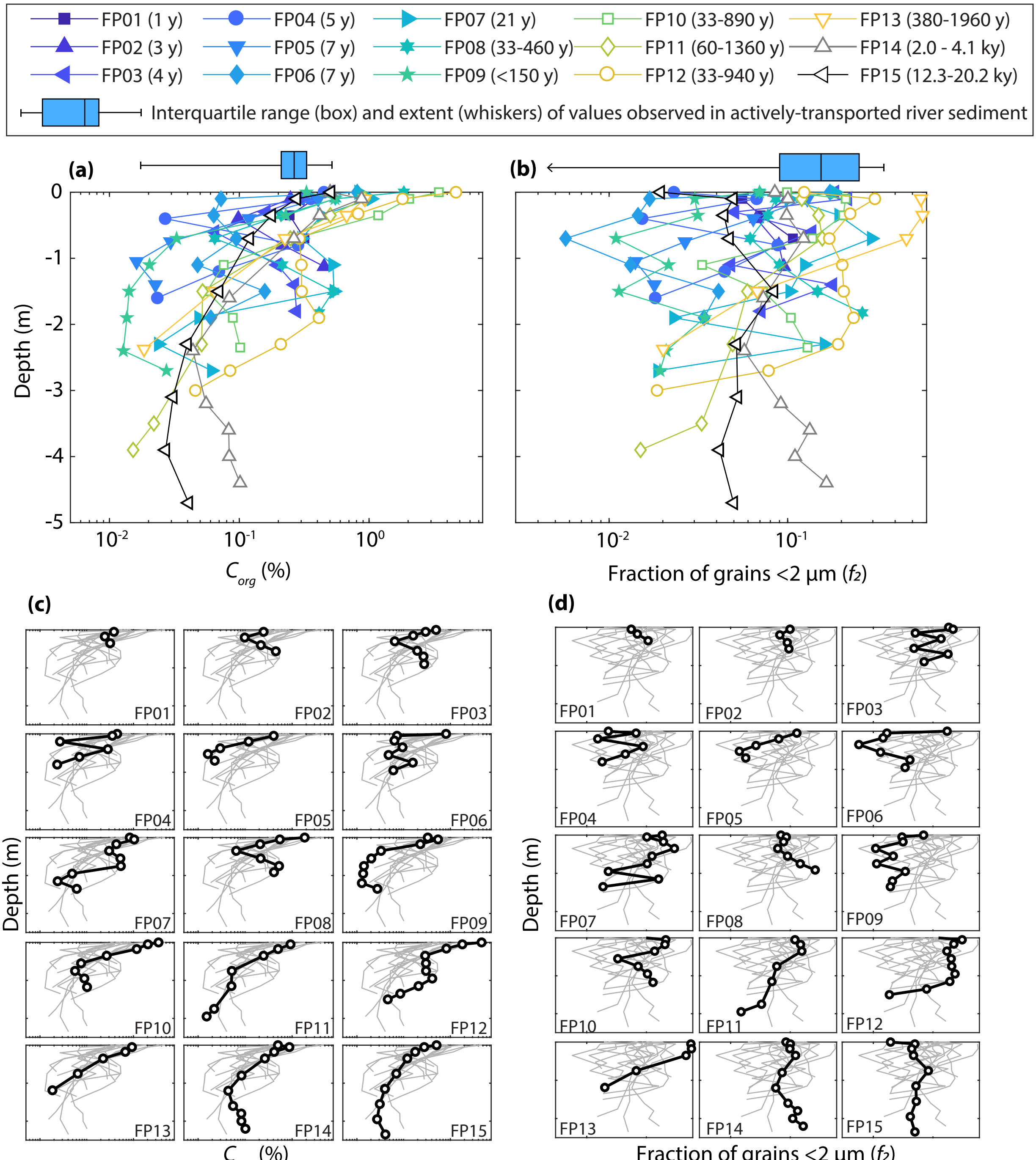

Figure 4: Floodplain depth profiles of POC weight percent (C_{org}) and fraction of grains less than 2 µm (f_2). (a and b) Show all profiles of C_{org} and f_2, respectively, on the same plot, color-coded by floodplain age. (c and d) Highlight individual profiles of C_{org} and f_2, respectively, for each floodplain core (black line) with profiles from other floodplain cores in gray. Axis extent of individual profiles in (c) and (d) match extent shown in (a) and (b), respectively. Error bars are removed for clarity, but are reported in Table S1. Box and whisker plots in (a) and (b) show median, inter-quartile range, and full extent of values observed in actively transported river sediments.

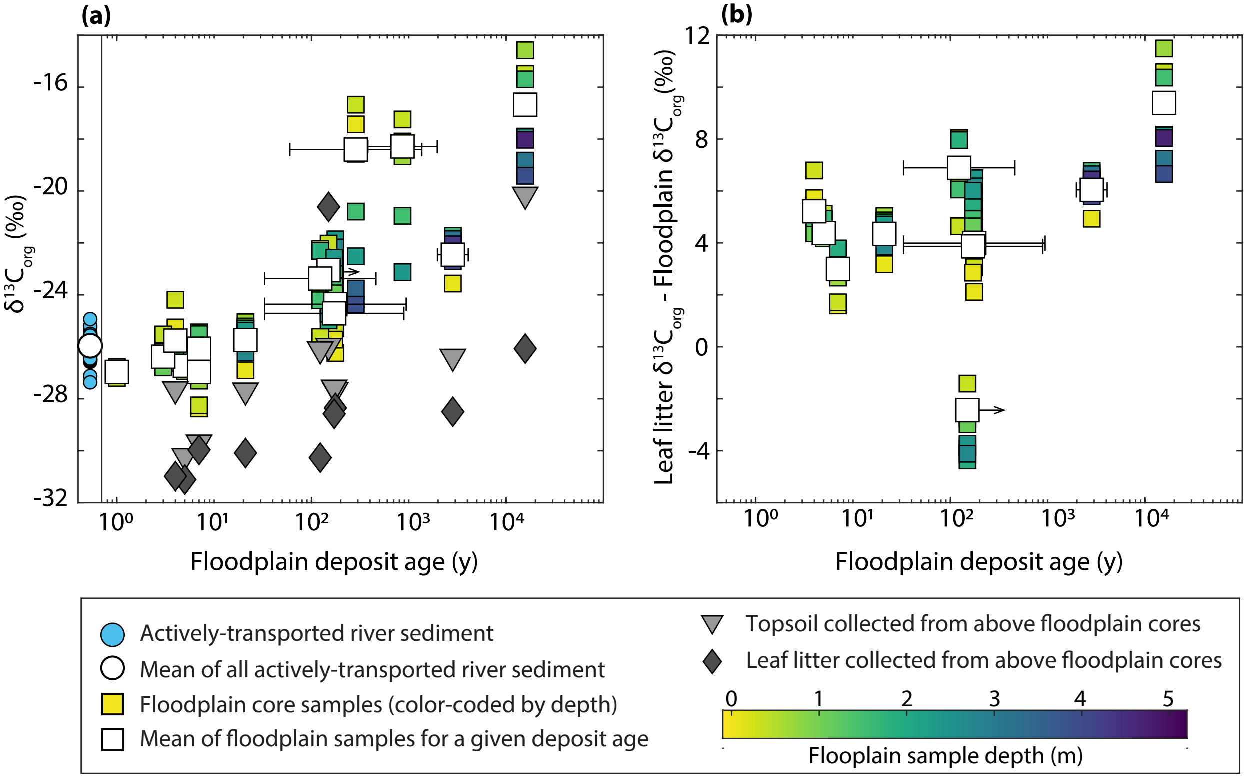

Figure 5: (a) Stable carbon isotope values of bulk POC ($\delta^{13}C_{org}$) from floodplain cores, top soil, and leaf litter versus independently constrained floodplain deposit age. Also shown are the $\delta^{13}C_{org}$ range of actively transported fluvial sediment in the Rio Bermejo (blue circles are individual samples, white circle is the mean of all values). (b) Difference between leaf litter and floodplain sample $\delta^{13}C_{org}$. In both panels floodplain samples are color-coded by depth below surface; white squares show concentration-weighted mean POC values with error bars indicating range in deposit age estimate. Error bars are smaller than the symbol where not shown. Right pointing arrow indicates unconstrained maximum depositional age of FP09.

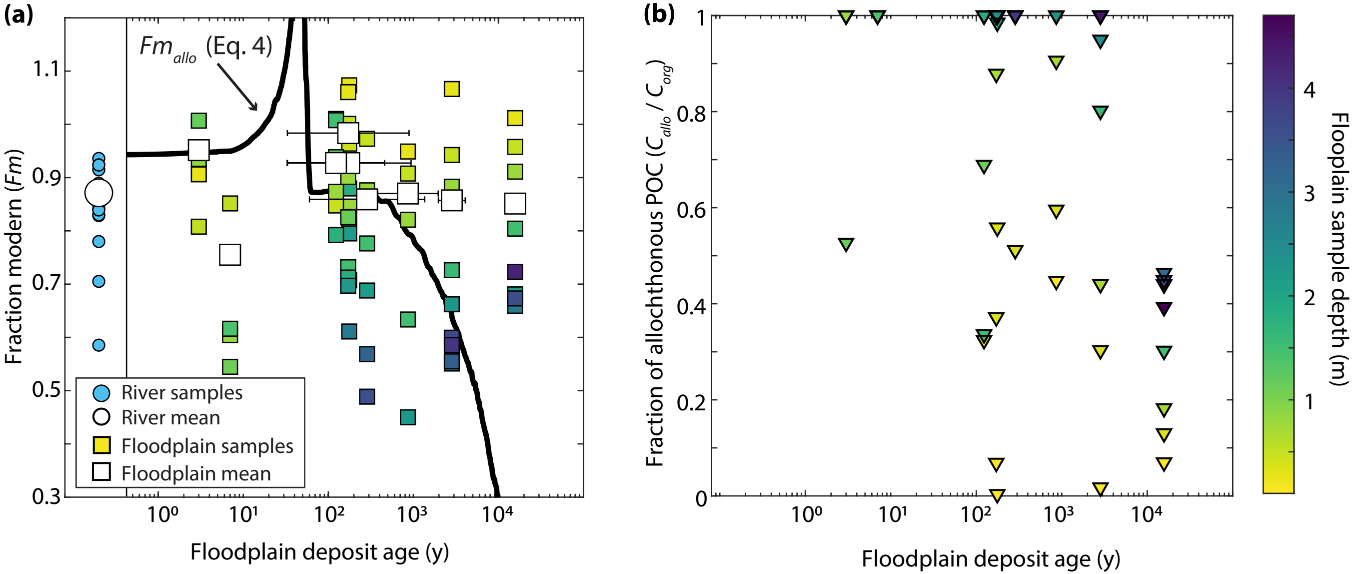

Figure 6: (a) Radiocarbon fraction modern (Fm) and (b) fraction of allochthonous POC (C_{allo}/C_{org}) in floodplain deposits as a function of independently-constrained floodplain depositional age. Symbols are color-coded by sample depth below the floodplain surface, with white squares in (a) showing POC concentration-weighted mean values for the entire floodplain core with error bars indicating the range in deposit age estimate (smaller than the symbol where not shown). Black line in (a) shows maximum possible Fm value for allochthonous POC (Fm_{allo}). Also shown in (a) is range of Fm values of river sediment (blue circles are individual samples and white circle is mean of all samples).

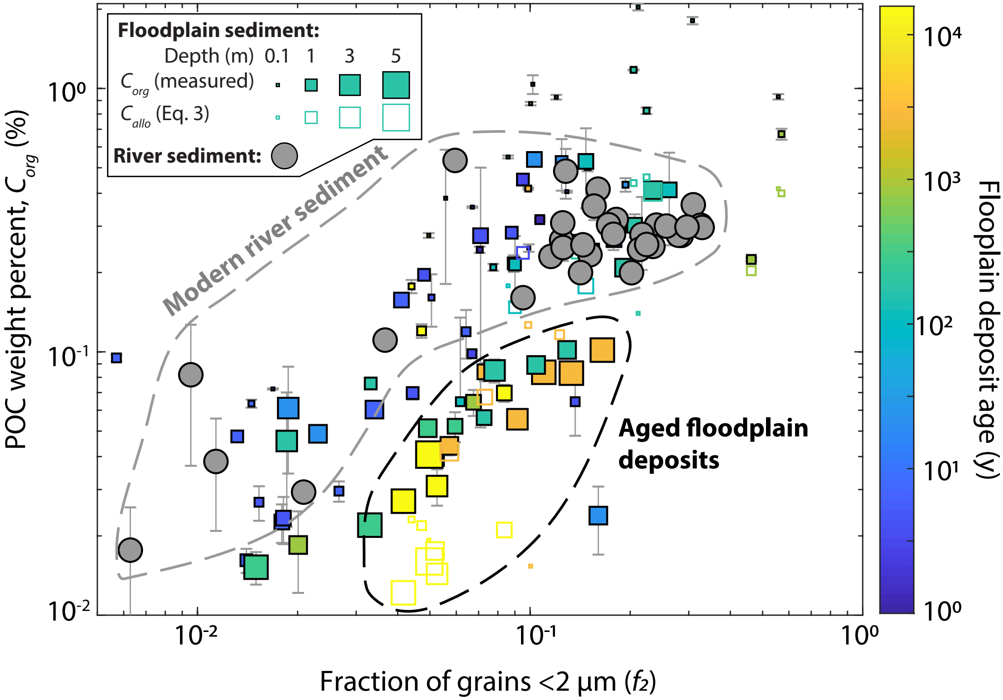

Figure 7: Comparison of POC weight percent (C_{org}) versus fraction of grains < 2 µm (f_2) for actively transported river sediment (gray circles) and floodplain deposits (squares). Floodplains deposits are color-coded by depositional age and symbol size indicates sample depth below surface. Solid squares show measured C_{org}, and open squares show calculated allocthonous POC (C_{allo}). In cases where $C_{org} = C_{allo}$, only solid squares are shown. Error bars show standard deviation from replicate measurements, and are smaller than the symbol size when not shown. Floodplain deposit FP09 is ommitted from the figure as we have only a minimum a constraint (150 y) on its age.